Life Sciences 270 (2021) 119122

Contents lists available at ScienceDirect

Life Sciences

journal homepage: www.elsevier.com/locate/lifescie

Extracellular vesicles derived from bone marrow mesenchymal stem cells repair functional and structural rat adrenal gland damage induced by fluoride

Eman Mohamed Faruk [a], Wardah Abdullah Alasmari [b], Hanan Fouad [c], Ola Elsayed Nafea [d,e,*], Rehab Abd Allah Hasan [f]

[a] Department of Histology and Cell Biology, Faculty of Medicine, Benha University, Benha, Egypt
[b] Department of Anatomy, Faculty of Medicine, Umm Al Qura University, Mecca, Saudi Arabia
[c] Medical Biochemistry and Molecular Biology, Faculty of Medicine, Cairo University, Giza, Egypt
[d] Department of Forensic Medicine and Clinical Toxicology, Faculty of Medicine, Zagazig University, Zagazig, Egypt
[e] Department of Clinical Pharmacy, College of Pharmacy, Taif University, Taif, Saudi Arabia
[f] Department of Histology and Cell Biology, Faculty of Medicine for Girls (AFMG), Al-Azhar University, Cairo, Egypt

ARTICLE INFO

Keywords:
Adrenal glands
Bone marrow mesenchymal stem cells
Corticosterone
Extracellular vesicles
Fluoride
Steroidogenesis

ABSTRACT

The adrenal glands have striking morpho-biochemical features that render them vulnerable to the effects of toxins. Aims: This study was conducted to explore the therapeutic utility of extracellular vesicles derived from bone marrow mesenchymal stem cells (BMSC-EVs) against fluoride-induced adrenal toxicity. Materials and methods: The work included isolation and further identification of BMSC-EVs by transmission electron microscopy and flow cytometric analysis. Adrenal toxicity in rats was induced by oral administration of 300 ppm of sodium fluoride (NaF) in drinking water for 60 days followed by a single dose injection of BMSC-EVs. The effects of BMSC-EVs against NaF was evaluated by adrenal oxidant/antioxidant biomarkers, hormonal assay of plasma adrenocorticotrophic hormone (ACTH) and corticosterone (CORT) and mRNA gene expression quantitation for adrenal cortical steroidogenic pathway-encoding genes. Histopathological examination of the adrenal tissue was performed. Key findings: BMSC-EVs were effectively isolated and characterized. NaF exposure decreased adrenal superoxide dismutase and catalase activities, increased adrenal malondialdehyde levels, elevated plasma ACTH, diminished CORT concentrations and downregulated the adrenal cortical steroidogenic pathway-encoding genes. In addition, NaF-induced marked adrenal histopathological lesions. Significance: BMSC-EVs treatment repaired damaged adrenal tissue and recovered its function greatly following NaF consumption. BMSC-EVs reversed the toxic effects of NaF and reprogramed injured adrenal cells by activating regenerative processes.

1. Introduction

The adrenal gland, in particular the cortex, is necessary for regulation of physiologically adaptive response to stressors and maintenance of body homeostasis [1]. The adrenal cortex is the most susceptible endocrinal organ to toxic insults. This can be explained by adrenal anatomical and biochemical characteristics, such as hypervascularity, lipophilicity due to rich cholesterol and steroid content allowing accumulation of lipid soluble xenobiotics as well as high content of unsaturated fatty acids and cytochrome P450 (CYP-450) enzymes system in adrenal cortex favoring damage by lipid peroxidation and oxidative stress. In addition, exposure to toxic compounds and drugs is considered a stressful event and activates hypothalamo–pituitary–adrenocortical (HPA) axis to increase adrenocorticotrophic hormone (ACTH) release. Overproduction of adrenocorticotropic (ACTH) hormone leads to structural and functional alteration of adrenal gland and its response to stressors [2–5].

Adrenocortical toxicity in humans can result in seriously diminished cortisol and aldosterone release. Along with the role glucocorticoid in overcoming overwhelming inflammation considered to be the most important action of glucocorticoids in the stress response [2]. Fluoride is still unavoidable environmental pollutant negatively influencing human health [6].

Fluoride ranked the 13th most abundant element in the Earth's crust.

* Corresponding author at: Faculty of Medicine, Department of Forensic Medicine and Clinical Toxicology, Zagazig University, Zagazig 44519, Egypt.
E-mail addresses: olanafea@zu.edu.eg, oenafea@tu.edu.sa (O.E. Nafea).

https://doi.org/10.1016/j.lfs.2021.119122
Received 2 December 2020; Received in revised form 10 January 2021; Accepted 18 January 2021
Available online 26 January 2021

Contaminated drinking water is the main source of human exposure to fluoride. According to the World Health Organization (WHO), approximately 200 million persons all over the world are drinking water with fluorine concentration above 1.5 mg/L [7]. Other sources include toothpastes, foods, water, coal, pesticides, bottled teas and fluorinated pharmaceuticals [8]. Albeit, fluoride is an essential trace element that plays a vital role in maintaining stability to teeth and bones, fluorosis/chronic exposure to fluoride more than 1 ppm causes hazardous health effects [9,10]. Many research studies focused on the toxic effects of fluoride in body organs such as skeleton, brain, GIT, kidney, liver. Up to date, the effects of fluoride on endocrine tissues has not been satisfactorily discovered, in particular steroid-producing tissues as adrenals [11–13].

Mesenchymal stem cells (MSCs) transplantation is considered as a promising tool for regenerative medicine. However, the weak engraftment and low survival rates are major problems that hinder its clinical applications [14]. In addition, allo-immune responses, tumorigenicity and pulmonary embolism are other possible complications in the clinical practice [15–19].

The mechanism of action of MSCs is not fully understood, it is suggested that MSCs secrete cytokines and trophic factors as well as extracellular vesicles (EVs) that may partially play a role in their therapeutic potentials. EVs simulate the phenotypes of the cells of origin as well as EVs could control stemness, renewal and differentiation of stem cells and their subpopulations [20–23].

EVs are a heterogeneous group of membrane-bound vesicles loaded with different bioactive molecules, including RNAs, DNAs, proteins, and lipids. EVs are classified into three main categories; exosomes, microvesicles (MVs), and apoptotic bodies. They regulate a wide range of biological activities either directly or indirectly. The active interaction of EVs with other cells controls various normal physiological and pathological conditions, such as malignancy, infection, and neurodegenerative diseases. EVs are currently considered as a novel way for intercellular communication, allowing cells to exchange proteins, lipids and genetic material [24–27].

We hypothesized that EVs derived from bone marrow mesenchymal stem cells (BMSC-EVs) can repair adrenal gland injury in rats after fluoride exposure. Accordingly, in this work to explore the potential alleviating effects of BMSC-EVs on fluoride induced rat adrenal gland toxicity, we studied the effects of BMSC-EVs on adrenal oxidant/antioxidant status, plasma concentrations of adrenocorticotrophic hormone (ACTH) and corticosterone (CORT) hormones, adrenocortical steroidogenic pathway-encoding genes; melanocortin 2 receptor accessory protein 2 (*MRAP2*), steroidogenic acute regulatory protein (*StAR*) and 11β-hydroxysteroid dehydrogenase-type 1 (*11β-HSD1*) and the associated histopathological lesions. To authors' knowledge, this is the first work exploring the therapeutic utility of BMSC-EVs against fluoride-induced adrenal toxicity.

2. Materials and methods

Preparation, isolation and identification of rat BM-MSCs and MSCs derived EVs were conducted in the Stem Cell Unit of Biochemistry and Molecular Biology at the Medical Biochemistry Department, Faculty of Medicine, Kasr Al-Ainy University, Egypt.

2.1. Preparation and isolation of BM-MSCs

Rats BM-MSCs were isolated from the femurs and tibias of six-week-old female albino rats and their body weights ranged from 150 to 200 g (Laboratory Experimental Animal House Unit of Al-Azhar University (Girls), Cairo, Egypt). In accordance with Local Ethical Committee for the experimental use of laboratory animals and the National Institutes of Health Guidelines. In brief, the rats were sacrificed by cervical dislocation and the bone marrows were flushed out with sterile phosphate buffered saline (PBS). After centrifugation, cells were resuspended in alpha-Minimum Essential Medium (MEM) supplemented with 10% selected fetal bovine serum and 80 μg/mL gentamicin and plated at a density of 1×10^6 nucleated cells/cm^2. Non-adherent cells were removed after 72 h by media change. When foci reached confluence, adherent cells were detached with 0.25% trypsin, 2.65 mM EDTA, centrifuged and sub-cultured at 7.000 cells/cm^2. After two subcultures, adherent cells were used for isolation of BMSC-EVs [28].

2.2. Preparation and isolation of EVs derived from rat-BM-MSCs

In brief, EVs were separated from the supernatants of second and third passages of MSCs. Centrifugation at 2000 $\times g$ for 20 min was done to remove the debris. Centrifugation at 100,000 $\times g$ for 1 h at 4 °C was done for the cell-free supernatant by using ultracentrifuge of Beckman Coulter Optima L-90 K (AQ11). The pellet was washed by serum-free medium and by N-2-Hydroxy Ethyl Piperazine-N′-2-Ethane Sulfonic acid (HEPES) 25 mM (Sigma Aldrich, USA), then an ultracentrifugation was employed for the second pellet under the same conditions. In addition, MSCs were tested by flow cytometry using specific surface markers (CD90, CD45, HLA-DR and CD34) [29].

2.2.1. Identification and detection of rat-BMSC-EVs

BMSC-EVs were labeled with fluorescent cell tracer PKH26 (Sigma, USA, MINI26) and injected into the caudal vein of NaF treated rats (group III). We used fluorescence microscope to examine the adrenal tissue to visualize homing of PKH26 stained EVs [30]. In addition, BMSC-EVs were tested by flow cytometry using specific surface markers (CD73, CD44, CD29 and CD63) [29].

2.3. Transmission electron microscopy (TEM) characterization for rat-BMSC-EVs

EVs were fixed with 2.5% glutaraldehyde for 2 h, after being washed, EVs were ultra-centrifuged and suspended in 100 μL human serum albumin (HSA). A total of 20 μL of EVs was loaded onto a formvar/carbon-coated grid, negatively stained with 3% aqueous phosphor-tungstic acid for 1 min and observed by TEM (HITACHI, H-7650, Japan), which showed their spheroid morphology and confirmed their nano-size [31].

2.4. Animals

The study included 21 female albino rats (150 to 200 g), their age ranged from six to eight weeks. The animals were bred and maintained in air-conditioned animal houses with specific pathogen-free conditions, and were subjected to 12 h light and dark cycles, and allowed free access to food and the tap water was supplied *ad libitum*. For acclimation purpose, the rats were handled manually for one week before the experiment to allow biological stabilization.

All animals received humane care in compliance with the Animal Care Guidelines of the National Institutes of Health (NIH), and the Research Ethics Committee of the Faculty of Medicine, Al-Azhar University, Cairo, Egypt, approved the design of the experiment.

2.4.1. Experimental design

Animals were randomly assigned into three groups of seven rats each: control, NaF and NaF+ BMSC-EVs groups.

Group I (negative control): Normal healthy rats.

Group II (NaF): Treated with 300 ppm of NaF in drinking water *ad libitum* for 60 days [6,32,33]. This route of exposure was selected to simulate human exposure to fluorinated water.

Group III (NaF+ BMSC-EVs): Treated with NaF as in group II then intravenously injected through the caudal vein with a single dose of BMSC-EVs (the dose was adjusted to 100 μg protein/suspended in 0.2 mL PBS) [34]. After 30 days, these rats were sacrificed. BMSC-EVs pellet protein content was quantified by Bradford method (BioRad, Hercules, CA, USA).

2.5. Samples collection

After finishing the treatment protocol, the rats were fasted overnight, then rats were anesthetized intraperitoneally with pentobarbital (60 mg/kg) [35] for blood samples collection from the retro-orbital venous plexus. Blood samples from each rat were collected in EDTA-containing tubes and plasma was separated after centrifugation at 3000 rpm for 15 min at 4 °C. The separated plasma was kept at −80 °C until analysis. After blood collection, the rats were killed by cervical dislocation; the adrenal glands of each rat were excised immediately for biochemical analyses and histological/histochemical analyses.

2.6. Biochemical analyses

2.6.1. Oxidant/antioxidant biomarkers assays

For biochemical estimations, 0.5 mg of each adrenal tissue samples were taken, ground with liquid nitrogen in a mortar. The ground tissues were then treated with 4.5 mL of PBS. The mixtures were homogenized on ice using an Ultra-Turrax homogenizer for 15 min. Homogenates were used for determination of the antioxidant [superoxide dismutase (SOD) and catalase (CAT)] enzymatic activities. Assay of (SOD) and (CAT) activities using commercially available kits according to manufacturer's recommendations (Thermofisher scientific, Cat No. EIASODC for SOD and Cat. No. EIACATC for CAT). Results were expressed as millimole per minute per milligram tissue (mmol/min/mg tissue). Adrenal malondialdehyde (MDA); lipid peroxidation biomarker, was assessed by the commercial kits supplied by Abcam (Cat. No. ab118970) according to manufacturer's recommendations. Results were expressed as nanomole per milligram tissue (nmol/mg tissue). All assays were conducted at room temperature in triplicate.

2.6.2. Hormonal assays

We assessed plasma concentrations of ACTH and CORT hormones by chemiluminescence based immunoassay using Siemens DPC Immulite®1000 (Siemens Medical Solutions Diagnostics, Los Angeles, CA, United States).

2.6.3. Assessment of genes expression by real time polymerase chain reaction (PCR)

We studied melanocortin 2 receptor accessory protein 2 (*MRAP2*), steroidogenic acute regulatory protein (*StAR*) and 11*β*-hydroxysteroid dehydrogenase-type 1 (*11β-HSD1*) in the rats' adrenal glands by real time PCR (qRT-PCR) using StepOnePlus™ real time PCR system (Applied Biosystems, USA). Total RNA was extracted from the tissue using RNeasy Mini Kit (Qiagen, USA, Cat No./ID: 74104). The extracted RNA was quantified by spectrophotometry (JENWAY, USA) at 260/280 nm. Primers sequences used in the qPCR measurements for *GAPDH*, *MRAP2*, *11β-HSD* and *StAR* are listed in Table 1. PCR primers were got from GenBank RNA sequences cited at the following website: http://www.ncbi.nlm.nih.gov/tools/primer-blast For the selection of the ideal primer pair, the considered factors included melting temperature (Tm: 60–65 °C) and applicant length of about 90–200 bp.

2.6.4. Real-time quantitative PCR using SYBR green

Expression of *MRAP2*, *StAR* and *11β-HSD1* genes were quantified with the StepOnePlus ™ Real-Time PCR system software version 3.1 (Applied Biosystems, CA, USA). Optimization of the annealing temperature was conducted for the PCR protocol and for the primer sets. All cDNAs were prepared for all gene markers, glyceraldehyde 3-phosphate dehydrogenase (*GAPDH*), and for non-template negative control. We used fixed concentrations (10.5 mg) of protein contents in the adrenal tissues. The fixed content of proteins was obtained from 30 to 36 mg tissue. RNA extraction yields 100 μg of RNA. Elution of RNA was done by 100 μL nuclease free water. The concentration of RNA was 100 μg/100 μL = 1.0 μg RNA/μL water. We used 5 μL RNA (contains 5 μg RNA) in reverse transcriptase reaction which yields fixed constant concentrations of cDNA. We used 3 μL cDNA that (contains 100 ng cDNA as recommended by the manufacturer) in SYBR green master mix. Five microliters of total RNA were used to generate cDNA using 20 pmol antisense primer and 0.8 μL AMV reverse transcriptase at 37 °C for 60 min. The relative abundance of mRNA species was evaluated using the SYBR® Green method (Applied Biosystems, CA, United States). Annealing temperature of 60 °C was optimized for all primer sets. Real time PCR was performed in 25 μL reaction volume consisting of Mater Mix of SYBR Green, 3 μL of cDNA, 900 nmol/L of every primer. Amplification conditions were conducted according to the manufacturer specifications: 2 min at 50 °C, 10 min at 95 °C, 40 repeated cycles with 15 s denaturation and 10 min of annealing/extension at 60 °C. This method is a well standardized routine technique in quantitative real time PCR.

Table 1
Oligonucleotide primers sequences used in the quantitative polymerase chain reaction (PCR) measurements for the *GAPDH*, *MRAP2*, *11β-HSD1* and *StAR*.

Gene	Primers sequences	GenBank® accession number
GAPDH	Forward: 5′-AGTGCCAGCCTCGTCTCATA-3′ Reverse: 5′- ACCAGCTTCCCATTCTCAGC-3′	NM_017008.4
11β-HSD1	Forward: 5′-TGAAATCCATCACGCAGGCT-3′ Reverse: 5′-ATAACTGCCGTCCAACAGGG-3′	NM_017080.2
MRAP2	Forward: 5′-AGCTGAAAGCCAACAAGCAC-3′ Reverse: 5′-GGTAGGCTTGGGGACTATGC-3′	NM_001135834.1
StAR	Forward: 3′-CGTCGGAGCTCTCTACTTGG-5′ Reverse: 3′-CCCAAGGCCTTTTGCATAGC-5′	NM_031558.3

Abbreviations; *GAPDH*, glyceraldehyde 3-phosphate dehydrogenase; *11β-HSD1*, 11*β*-hydroxysteroid dehydrogenase-type 1; *MRAP2*, Melanocortin 2 receptor accessory protein 2; *StAR*, Steroidogenic acute regulatory protein.

2.6.4.1. Calculation of relative quantification (relative expression). We calculated relative gene expressions of all assessed genes using the comparative Cycle threshold (Ct) method [36]. PCR data results show Ct values of the target genes and the housekeeping gene (*GAPDH*). A negative control sample was that no template cDNA used. Data were calculated using StepOnePlus™ real time PCR system (Applied Biosystems, CA, USA). All values were normalized to *GAPDH* housekeeping gene and expressed as fold changes relative to the background levels found in the control samples.

2.7. Histological analyses

The adrenal specimens were fixed in 10% buffered formalin solution for 24 ~ 48 h, dehydrated in escalating grades of ethanol and embedded in paraffin. Serial sections of 3 ~ 5 μm thickness were cut a by rotary microtome (LEICA RM 2125; UK) and subjected to the followings:

2.7.1 Fluorescence detection (to detect PKH26-labeled BMSC-EVs) by fluorescent microscope in unstained paraffin sections [30].

2.7.2 Hematoxylin and eosin (H&E) stain for histological assessment [37].

2.7.3 Periodic Acid Schiff (PAS) stain is used to detect polysaccharides e.g., glycogen [38].

2.7.4 Mallory trichrome stain for collagen fibers detection [39].

2.8. Immunohistochemical analysis

Immunohistochemichal staining for proliferating cell nuclear antigen (PCNA): The adrenal specimens for immunostaining required

pretreatment, this was achieved by boiling for 10 min in 10 Mm, pH 6 citrate buffer for antigen retrieval and leaving the sections to cool in room temperature for 20 min. Then, the sections were incubated for 1 h with the primary antibodies (rabbit polyclonal antibody; Lab Vision Corporation Laboratories, diluted 1:100, catalogue number PA5-27214). The usual of avidin-biotin peroxidase method was conducted by using diamino-benzidin (DAB) for positive detection and Mayer's hematoxylin for counterstaining. Negative controls were prepared with exclusion of the primary antibody [40].

2.9. Histo-morphometric measurements

We used Image-Pro Plus program (version 6.0; Media Cybernetics Inc., Bethesda, Maryland, USA) for histo-morphometric assessment, in the Pathology Department, Faculty of Medicine, Cairo University. Five randomly selected high-power microscopic fields were inspected for counting the numbers of PCNA positive cells. Also, the area percentage of Mallory trichrome-stained collagen fibers, PAS polysaccharide substances were examine at ×20 and, the mean thickness of the whole adrenal cortex and the thickness of each zona of the adrenal cortex were examined at × 10 magnification, and the results were expressed as mean area % of collagen/μm^2 and PAS polysaccharide substances.

2.10. Statistical analysis

Continuous variables were presented as mean ± standard deviation (SD). We used Shapiro–Wilk test to assess the normality of the continuous variables. Bartlett's test was used to check the equality of variance. According to the equality of variance, we used ordinary one one-way analysis of variance (ANOVA) or Welch's ANOVA test detect statistical differences between groups. Post-hoc tests (Bonferroni test if equal variances were assumed; Tamhane T2 test if equal variances were not assumed) were performed for multiple comparisons between the experimental groups. Differences were considered significant at a $P < 0.05$. All statistical comparisons were two-tailed and performed using Graphpad Prism, Version 8.0 Software (GraphPad Software; SanDiego, CA, USA).

3. Results

3.1. Identification of rat-BMSC-EVs

To assess the therapeutic role of rat-BMSC-EVs against NaF-induced rat adrenal gland toxicity, the isolated rBMSCs derived-EVs were examined under TEM. Their spheroid morphology with approximately 50 to 1000 nm size were shown (Fig. 1a, b). BMSC-EVs were then recognized by detecting surface markers including CD73, CD44, CD29 and CD63 (> 90% of EVs were positive) by the flow cytometry analysis (Fig. 1c, d). PKH26-labeled EVs appeared as red fluorescent cells before injection to NaF treated rats (Fig. 1e) and within the adrenal tissue after single dose of BMSC-EVs (Fig. 1f).

3.2. BMSC-EVs restored adrenal oxidant/antioxidant balance following NaF treatment

We assessed SOD and CAT enzymatic activities as well MDA levels in adrenal tissues to verify the alleviating effect of BMSC-EVs against oxidative stress of NaF-induced adrenal toxicity. We found that adrenal SOD and CAT activities significantly diminished in NaF treated rats compared with control rats (698.20 ± 20.75 vs 1189.0 ± 16.47 mmol/min/mg tissue, $P < 0.001$ and 70.28 ± 5.49 vs 121.50 ± 9.42 mmol/min/mg tissue, $P < 0.001$, respectively). While adrenal MDA levels significantly elevated in NaF treated rats compared to control rats (4.23 ± 0.48 vs 1.58 ± 0.38 nmol/mg tissue, $P < 0.001$). BMSC-EVs caused significant increase in adrenal SOD and CAT activities with significant decrease in adrenal MDA levels compared with NaF treated rats (846.8 ± 10.60 Vs 698.20 ± 20.75 mmol/min/mg tissue, $P < 0.001$, 86.20 ± 6.73 vs 70.28 ± 5.49 nmol/mg tissue, $P = 0.02$ and 2.23 ± 0.21 vs 4.23 ± 0.48 nmol/mg tissue, $P < 0.001$, respectively) (Fig. 2a).

3.3. BMSC-EVs failed to diminish plasma ACTH but elevated CORT concentration following NaF treatment

Plasma ACTH concentration significantly elevated in NaF treated group and BMSC-EVs treated rats compared with control group (3.36 ± 0.76 vs 1.72 ± 0.87 ng/mL, $P = 0.020$ and 2.98 ± 0.11 vs 1.72 ± 0.87 ng/mL, $P = 0.024$, respectively). However, plasma CORT concentration significantly diminished in NaF treated group compared with control rats. BMSC-EVs treatment significantly elevated plasma CORT concentration following fluoride exposure (22.39 ± 0.31 vs 19.38 ± 0.79 μg/dL, $P < 0.001$, respectively) (Fig. 2b).

3.4. BMSC-EVs upregulated StAR and 11β-HSD1 mRNA expression but not MRAP2 following NaF treatment

BMSC-EVs significantly upregulated the expression levels of *StAR* and *11β-HSD1* (0.90 ± 0.05 vs 0.78 ± 0.03-fold change, $P = 0.014$ and 0.96 ± 0.077 vs 0.60 ± 0.046-fold change, $P = 0.004$, respectively) compared with NaF treated groups. NaF treatment significantly downregulated the expression levels of *MRAP2*, *StAR*, and *11β-HSD1* compared with control rats ($P < 0.001$ for each) (Fig. 2c).

3.5. BMSC-EVs reversed rat adrenal histological lesions induced by NaF treatment

Examination of H&E-stained sections from the control rats' adrenal gland revealed the thick connective tissue covering capsule. The parenchyma of the gland was formed of outer cortex and inner medulla. The cortex included from outside to inside, rounded or arched clusters of zona glomerulosa (ZG) cells under the capsule. Then followed by large, polyhedral frothy or pale vacuolated acidophilic cells with vesicular rounded nuclei arranged in columns and longitudinal cords of one or two cells of the zona fasciculate (ZF) with blood sinusoids in between. Finally, branched anastomosing cords of zona reticularis (ZR) cells with blood sinusoids in between the cords. The cells of this zone were small, deeply stained and closely packed. The medulla consisted of anastomosing cords of secretory cells grouped around wide blood sinusoids. These cells were large polyhedral with basophilic cytoplasm (Fig. 3a–c). NaF treatment apparently decreased the cortical thickness with loss of architecture and orientation of ZG, ZF and ZR. ZG cells appeared vacuolated with small darkly stained nuclei. ZF cells appeared darkly stained with deeply stained nuclei. ZR cells could be demonstrated with vacuolated cytoplasm and small deeply stained nuclei. The anastomosing cords of the medulla appeared widely separated with multiple dilated and congested blood sinusoids in between. Some cells of the medulla were shrunken (Fig. 3d–h). BMSC-EVs treatment showed more or less a picture similar to that of the control group (Fig. 3i, j).

3.6. BMSC-EVs increased the adrenocortical thickness following NaF treatment

BMSC-EVs treatment significantly increased the whole adrenocortical thickness with its three layers compared with NaF treated rats ($P < 0.001$) (Fig. 3k).

3.7. BMSC-EVs restored carbohydrate depletion induced by NaF in rat adrenal tissues

In order to assess the distribution of carbohydrate contents in adrenal tissues, we stained sections of adrenal gland in all groups by PAS stain. In the control group, adrenal gland showed a strong positive reaction of carbohydrate distribution in the capsule, cortex, and medulla (Fig. 4a,

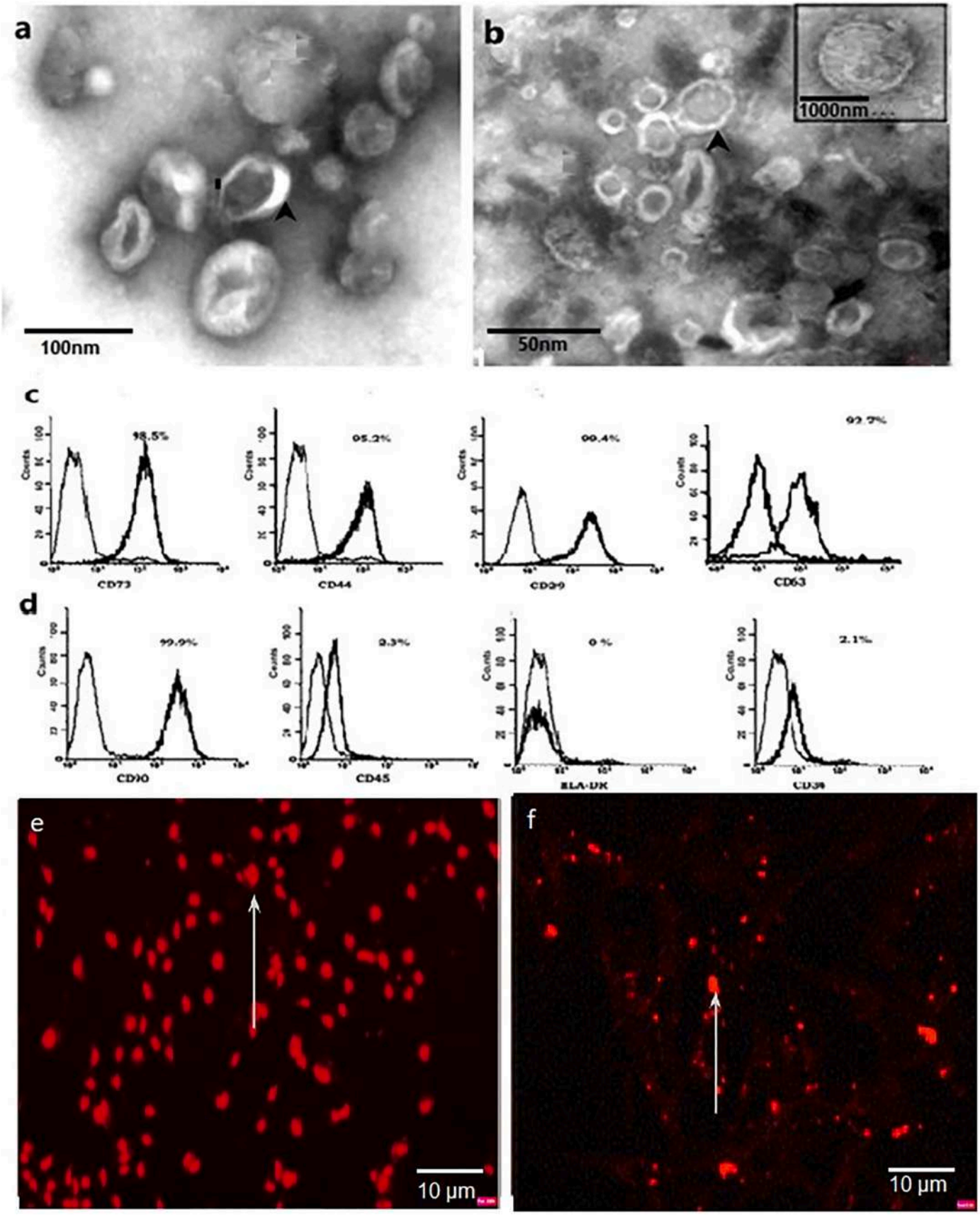

Fig. 1. Identification of BMSC-EVs. a, b Identification of BMSC-EVs by TEM show the spheroid shaped vesicles at the diameter of around (50 to 1000 nm). c, d The cytofluorimetric analysis of BMSCs and BMSC-EVs. c BMSC-EVs were positive for CD73, CD44, CD29 and CD63. d BMSCs were positive for CD90, and negative for CD45, HLA-DR and CD34. e, f 2. BMSC-EVs homing. e BMSC-EVs labeled with PKH26 red fluorescent dye in vitro (arrows). ×1000. f BMSC-EVs labeled with PKH26 red fluorescent dye in vivo (arrows). ×1000.

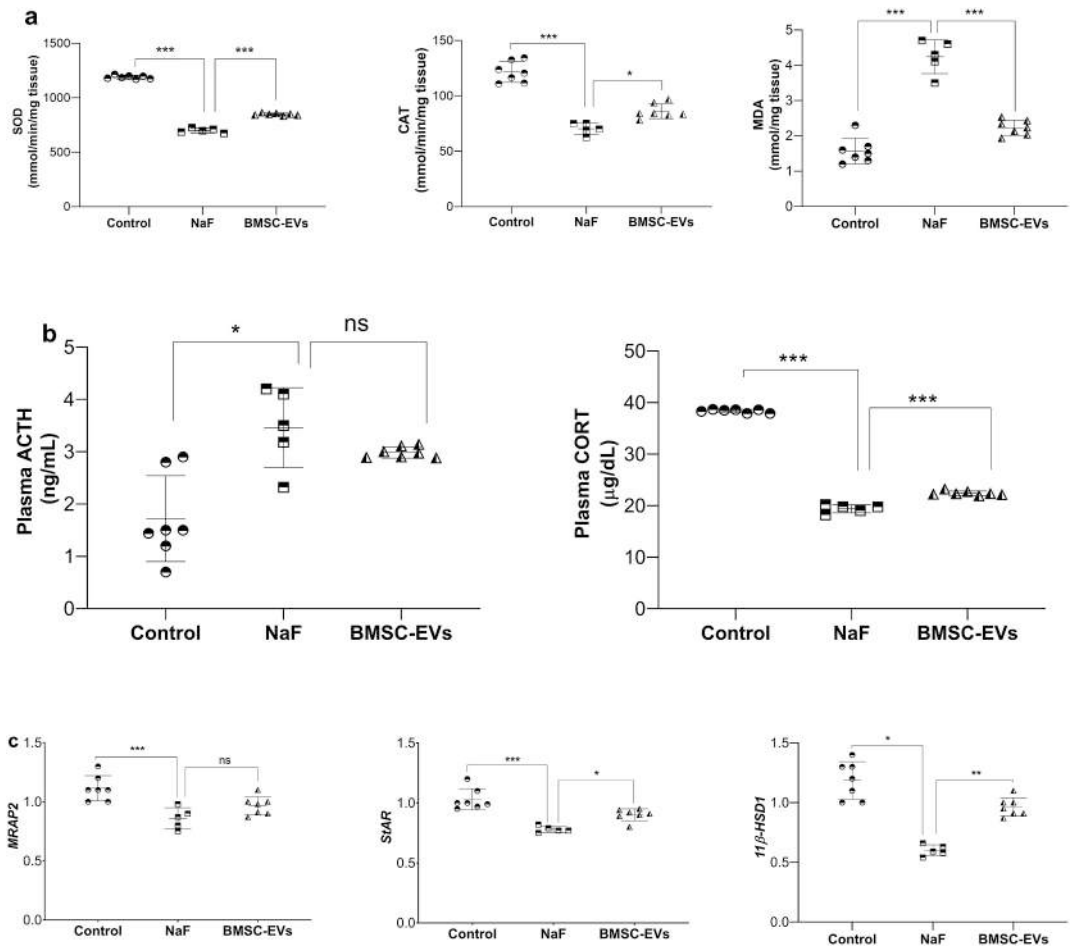

Fig. 2. Scatter dot plots showing the effects of BMSC-EVs on biochemical parameters in the rat sodium fluoride (NaF)-induced adrenal toxicity model. a oxidant/antioxidant biomarkers, A-one-way ANOVA test followed by post hoc Bonferroni's multiple comparisons test. b plasma ACTH and CORT concentrations, Welch's ANOVA followed by post hoc Tamhane's T2 multiple comparisons test and one-way ANOVA test followed by post hoc Bonferroni's multiple comparisons test, respectively. c adrenocortical steroidogenic pathway-encoding genes, statistical analyses for *MRAP2* and *StAR* results were performed by one-way ANOVA test followed by post hoc Bonferroni's multiple comparisons test while statistical analysis for 11β-*HSD1* results was performed by Welch's ANOVA followed by post hoc Tamhane's T2 multiple comparisons test. Horizontal lines represent the mean and error bars represent the standard deviation. $n = 7$ but two rats expired in NaF group. ns, a non-significant difference*$P < 0.05$, **$P < 0.001$ and ***$P < 0.001$. Control group (circles), NaF group (squares) and BMSC-EVs group (triangles). Abbreviations; SOD, superoxide dismutase; CAT, catalase; MDA, malondialdehyde; ACTH, adrenocorticotrophic hormone; CORT, corticosterone; *MRAP2*, melanocortin 2 receptor accessory protein 2; *StAR*, steroidogenic acute regulatory protein; *11β-HSD1*, 11β-hydroxysteroid dehydrogenase-type 1.

b), while in NaF group, a weak reaction of carbohydrate distribution in the capsule, cortex, and medulla was shown (Fig. 4c, d). BMSC-EVs treatment showed marked increase in positivity of PAS stain (Fig. 4e). Morphometric analysis of adrenal glands showed that the mean area percent of adrenal PAS significantly decreased in NaF group compared with control group (14.02 ± 0.01 vs 24.16 ± 0.10, $P < 0.001$) while BMSC-EVs treatment significantly increased the mean area percent of adrenal PAS compared with NaF group (21.17 ± 0.12 vs 14.02 ± 0.01, $P < 0.001$) (Fig. 4f).

3.8. BMSC-EVs reduced NaF-induced adrenal fibrosis in rats

In order to assess the degree of collagen deposition in adrenal tissues, we stained sections of adrenal gland in all groups by Mallory's trichrome stain. In the control group, adrenal gland showed collagen fibers deposition in capsule and parenchyma of glands (Fig. 5a) while in NaF group, a severe collagen connective tissue fibers deposition in capsule and parenchyma of glands was shown (Fig. 5b). BMSC-EVs treatment caused mild to moderate decreasing in collagen connective tissue fibers distribution (Fig. 5c). Morphometric analysis of adrenal glands showed that the mean area percent of adrenal collagen fibers disposition significantly increased in NaF group compared with control group (19.19 ± 0.11 vs 2.15 ± 0.32 μm^2, $P < 0.001$) while BMSC-EVs treatment significantly decreased the mean area percent of adrenal collagen fibers deposition compared with NaF group (8.21 ± 0.22 vs 19.19 ± 0.11 μm^2, $P < 0.001$) (Fig. 5d).

3.9. BMSC-EVs reversed the antiproliferative effect of NaF in rat adrenal tissue

In order to assess the degree of cellular proliferation of adrenal tissues, we stained sections of adrenal gland in all groups by PCNA immunohistochemical stain. In the control group, adrenal gland showed a positive immunoreaction in the nuclei of most of the parenchymal cells (Fig. 5e). While in NaF group, an apparent decrease in the number of positive cells was shown (Fig. 5f). BMSC-EVs treatment showed many immune-stained parenchymal cells for PCNA (Fig. 5g). Morphometric analysis of adrenal glands showed that the mean number of adrenal PCNA immune-positive nuclei significantly decreased in NaF group compared with control group (20.05 ± 0.06 vs 62.31 ± 1.32 cells, $P <$

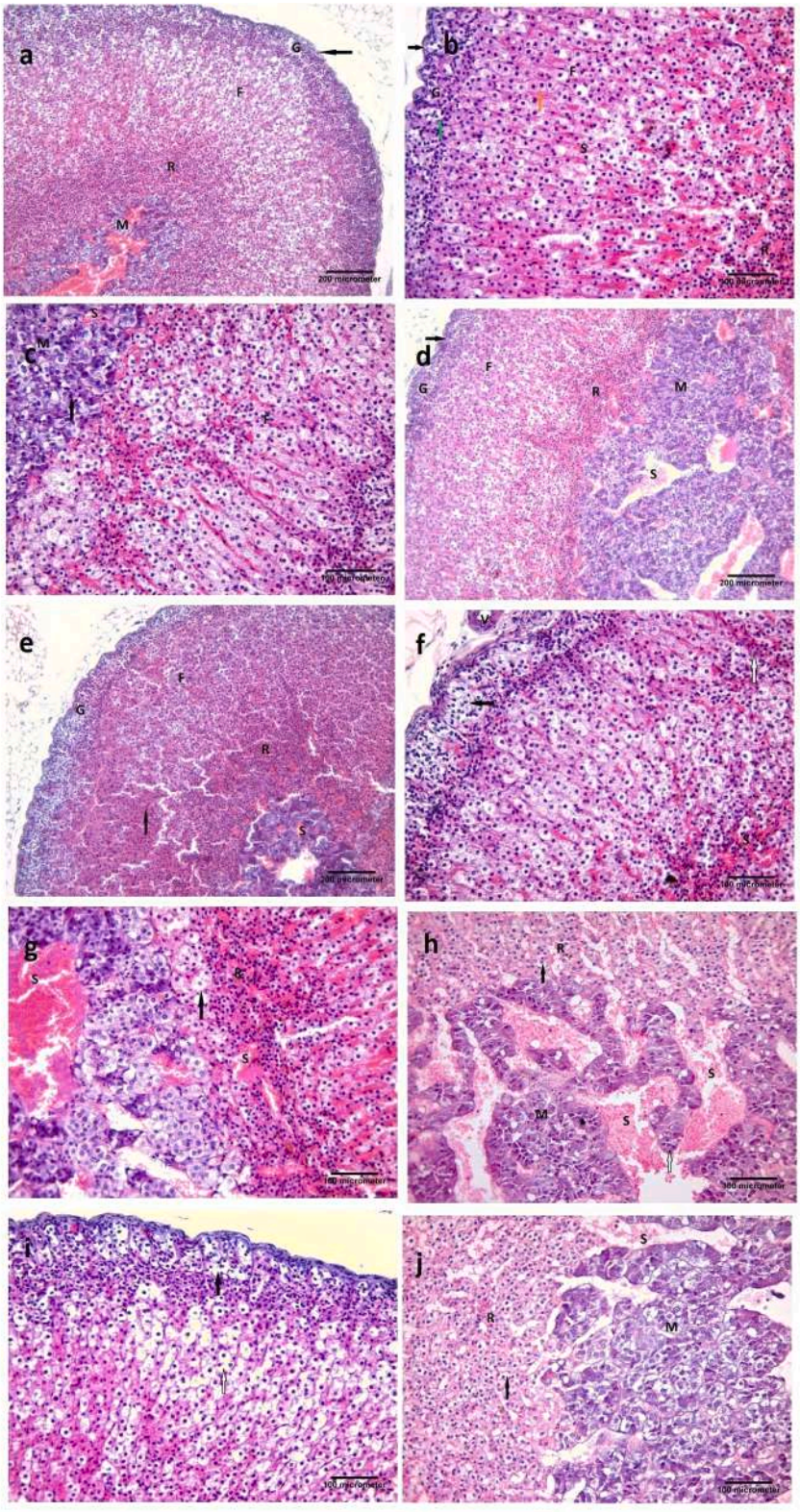

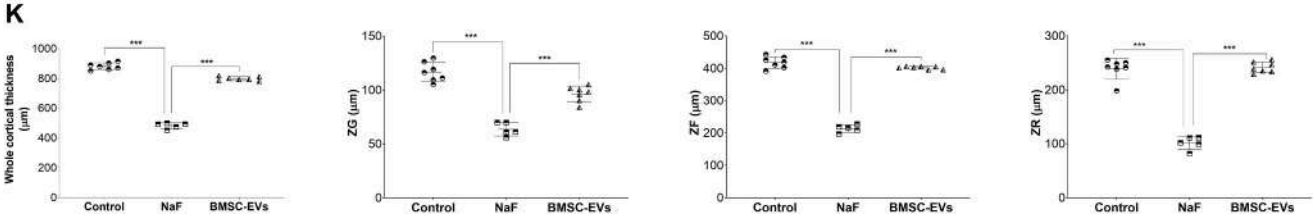

(caption on next page)

Fig. 3. Hematoxylin and eosin (H&E) stained sections of adrenals of the study groups:
a Control group showing the thick C.T capsule (arrow), underlying arches of zona glomerulosa (G), columns of zona fasciculata (F), branching cords of zona reticularis (R) and highly vascular medulla (M). H&E, × 100. b Control group showing the thick C.T capsule (black arrow), arched clusters of closely packed cells with spherical densely stained nuclei (green arrow) of zona glomerulosa cells (G), large, frothy appearance of acidophilic cells (orange arrow) arranged in longitudinal cords of the zona fasciculate (F) with blood sinusoids in between (S) and branched anastomosing cords of zona reticularis (R) with blood sinusoids in between the cords. The cells of this zone were small, deeply stained and closely packed. H&E, × 200. c control group showing the longitudinal cords of zona fasciculata (F). Also, the medulla (M) can be seen with basophilic polyhedral cells and vesicular nuclei arranged in anastomosing cords with blood sinusoids in between H&E, ×200. d NaF treated group showing apparent decrease in cortical thickness with loss of architecture of the zona glomerulosa (G). zona fasciculata (F) and zona reticularis (R) can be seen. Notice, vascular congestion in both zona reticularis and medulla (S) and thick capsule (arrow). H&E, × 100. e NaF treated group showing loss of architecture and orientation of the zona glomerulosa (G), zona fasciculata (F) and zona reticularis (R). the zona fasciculata cells (arrow) appear darkly stained with deeply stained nuclei. Notice, multiple congested blood sinusoids (S). H&E, × 100. f NaF treated group showing zona glomerulosa cells appear vacuolated with small darkly stained nuclei (black arrows), some zona fasciculate cells appear darkly stained with small darkly stained nuclei (white arrows). Dilated blood sinusoids (S) can be seen. Notice congested blood vessels (V). H&E, × 200. g NaF treated group multiple dilated blood sinusoids (S). Some cells near zona reticularis appear with vacuolated cytoplasm and darkly stained nuclei (arrow). H&E, × 200. h NaF treated group showing zona reticularis cells (R) with vacuolated cytoplasm and small deeply stained nuclei (black arrow). The anastomosing cords of the medulla (M) appear widely separated with multiple dilated and congested blood sinusoids (S) in between. Some cells of the medulla appear shrunken (white arrow). H&E, × 200. i BMSC-EVs treated group, the histological structure as nearly as the control group. H&E, × 200. j BMSC-EVs treated group, the histological structure as nearly as the control group. Notice, small dilated blood sinusoid (S) in the medulla (M). H&E, × 200.
k Scatter dot plots showing the effects of BMSC-EVs on the adrenal cortex and its three layers in the rat sodium fluoride (NaF)-induced adrenal toxicity model, statistical analyses for the whole adrenal cortical thickness, ZG and ZR morphometric results were performed by one-way ANOVA test followed by post hoc Bonferroni's multiple comparisons test while statistical analysis for ZF morphometric results was performed by Welch's ANOVA followed by post hoc Tamhane's T2 multiple comparisons test. Horizontal lines represent the mean and error bars represent the standard deviation. $n = 7$ but two rats expired in NaF group. Control group (circles), NaF group (squares) and BMSC-EVs group (triangles). Abbreviations; ZG, zona glomerulosa; ZF, zona fasciculata; ZR, zona reticularis. $^{***}P < 0.001$. (For interpretation of the references to colour in this figure legend, the reader is referred to the web version of this article.)

0.001) while BMSC-EVs treatment significantly increased mean number of adrenal PCNA immune-positive nuclei compared with NaF group (45.92 ± 0.19 cells vs 20.05 ± 0.06, $P < 0.001$) (Fig. 5h).

4. Discussion

The adrenals have striking morpho-biochemical characteristics that render them vulnerable to the effects of toxins and chemicals. Being endocrine glands, any functional alteration by either internal or external trigger will negatively influence the gland itself along with other body organs [5].

We found that exposure to 300 ppm of NaF in drinking water for 60 days in rats induced functional and morphological adrenal gland changes; NaF exposure decreased adrenal SOD and CAT activities with increased adrenal MDA levels, elevated plasma ACTH but diminished CORT concentrations, downregulated the adrenocortical steroidogenic pathway-encoding genes. In addition to degenerative structural adrenal changes, marked adrenal collagen depositions, strong antiproliferative changes as well as adrenal carbohydrates depletion. BMSC-EVs treatment repaired damaged adrenal tissue and recovered its function greatly following NaF consumption.

Fluoride negatively affects health via metabolic disarrangements by interfering with different cellular aspects including, but not limited to, gene expression, hormonal secretion, and oxidative stress [41].

Under normal circumstances, a balance between reactive oxygen species (ROS) production and ROS elimination exists; yet, oxidative stress denotes an imbalance due to an overproduction of ROS [42]. Our results showed that fluoride consumption decreased antioxidant biomarkers (SOD and CAT enzymatic activities) in rats' adrenal tissues with increased oxidative stress biomarker (MDA) levels. The present findings complement these former studies that verified the oxidative stress damage as a key mechanism of fluoride induced toxicity of various organ [33,43,44]. EVs restored adrenal oxidant/antioxidant balance following fluoride consumption. In corroboration, Keshtkar and coworkers [45], stated that a reduction of oxidative stress is the core therapeutic benefit of MSC-derived EVs in recovery of many organ injuries. In support, Bodart-Santos and colleagues [46], showed that the protective effect MSC-EVs against neuronal damage in Alzheimer's disease through inhibition of oxidative stress-induced injury of hippocampal neurons.

Adrenal gland is one of the steroid-producing tissues. During steroidogenesis, the movement of cholesterol from the outer to the inner mitochondrial membrane is considered as the rate-limiting event which is mediated by *StAR* protein [47]. While *11β-HSD1* is the principle enzyme that triggers the intracellular conversion of cortisone to physiologically active CORT in rats [48,49]. CORT is the primary adrenal corticosteroid in experimental rats [50]. Our findings revealed that BMSC-EVs significantly upregulated the expression levels of *StAR* and *11β-HSD1* following fluoride consumption with subsequent elevation of plasma CORT.

In general, melanocortin receptor accessory proteins (MRAP) are essential for melanocortin receptor type 2 (MC2R) or ACTH receptors to be successfully expressed on the adrenocortical cell surface, to form a high affinity binding pocket for ACTH [51,52]. MC2R/ACTH receptor is an exceptional among melanocortin receptors since it is only stimulated by ACTH in adrenocortical cells. *MRAP2* is critical for trafficking and function of ACTH receptor [53]. Heavy fluoride exposure can result in gene expression changes [54]. Pituitary glands release ACTH in stressful conditions, which in turn prompts increased synthesis of corticosteroids in adrenal cortex [55,56]. However, our findings displayed that fluoride strongly elevated plasma concentration of ACTH but diminished CORT. Das and Susheela reported that the chronic exposure to fluoride was associated with a decline in cortisol/CORT concentrations in human and animal studies [57]. Histologically, fluoride caused degenerative changes and fibrosis in adrenal cortex, with its three layers, specifically ZF with the resultant decline of glucocorticoids secretion. Also, the elevated ACTH can be elucidated by the feedback inhibition of HPA axis by the decreased CORT [58] as well as the decreased the adrenal *MRAP2* gene expression following NaF consumption.

The deleterious effects of NaF on adrenal gland structure could be attributed to fluoride induced oxidative stress injury. Consistently, Ghosh et al. [58] linked fluoride-induced testicular structural damage to ROS act.

Our results showed that NaF is associated carbohydrate depletion as documented by PAS stained adrenal sections. Adrenal gland insufficiency is associated with disturbance of carbohydrates metabolism [59,60].

In our study, EVs reversed adrenal collagenous fibers deposition provoked by fluoride. In corroboration, Grange et al. [61] revealed the ability of EVs to revert fibrosis of progress in renal tissue in diabetic mice.

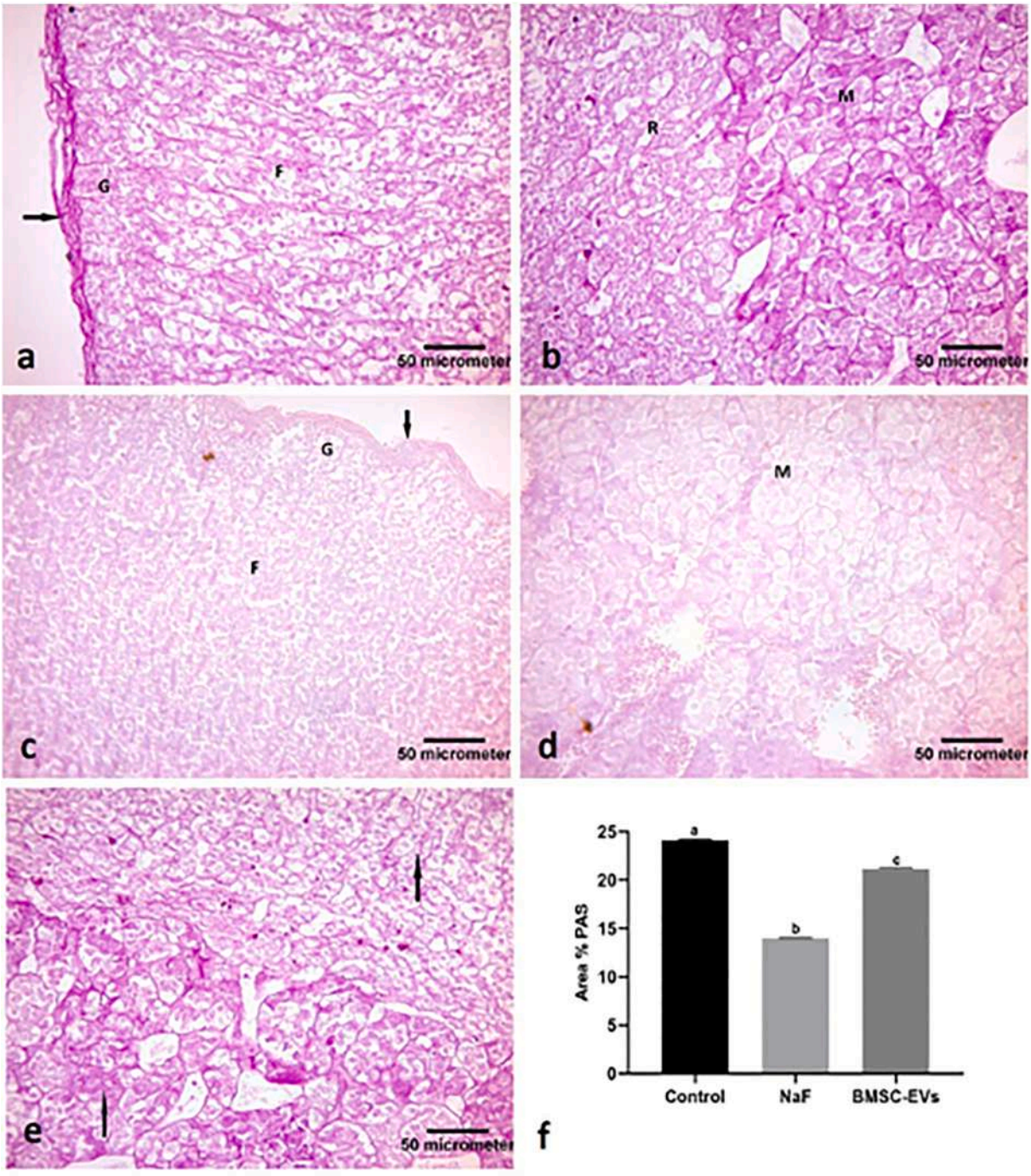

Fig. 4. Periodic Acid Schiff (PAS) stained sections of adrenals of the study groups:
a Control group showing a strong positive reaction of distribution of carbohydrate in the capsule (arrow) and zona glomerulosa (G), zona fasciculata (F). PAS, × 400. b Control group showing a strong positive reaction of PAS in zona reticularis cells (R) and the medulla (M). PAS, × 400. c NaF treated group showing a weak reaction of PAS in the capsule (arrow) and zona glomerulosa (G), zona fasciculata (F). PAS, × 400. d NaF treated group showing a weak reaction of PAS in the medulla (M) PAS, × 400. e BMSC-EVs treated group showing a strong PAS reaction (arrows). PAS, × 400. f Effects of BMSC-EVs on area percent of PAS of the adrenals in the rat sodium fluoride (NaF)-induced adrenal toxicity model. Data are mean ± standard deviation, $n = 7$ but two rats expired in NaF group. Bars not sharing the common superscript letters differ significantly at $P < 0.001$ by Welch's ANOVA followed by post hoc Tamhane's T2 multiple comparisons test.

PCNA is a Key intranuclear polypeptide that plays a fundamental role in DNA replication, excision and repair. Its synthesis and expression are related to cell proliferation [62]. We found that fluoride had an anti-proliferative effect on adrenal tissue as evidenced by low expression of PCNA. A single IV injection of EVs effectively increased proliferation of adrenal tissue following NaF consumption in rats. Likewise, MSC-EVs showed proliferative potentials in many tissue injuries, both in vivo and in vitro studies [63–65].

In contrast to our results, prior studies reported that adrenal glands are the least affected endocrine organs by the toxicity of fluoride

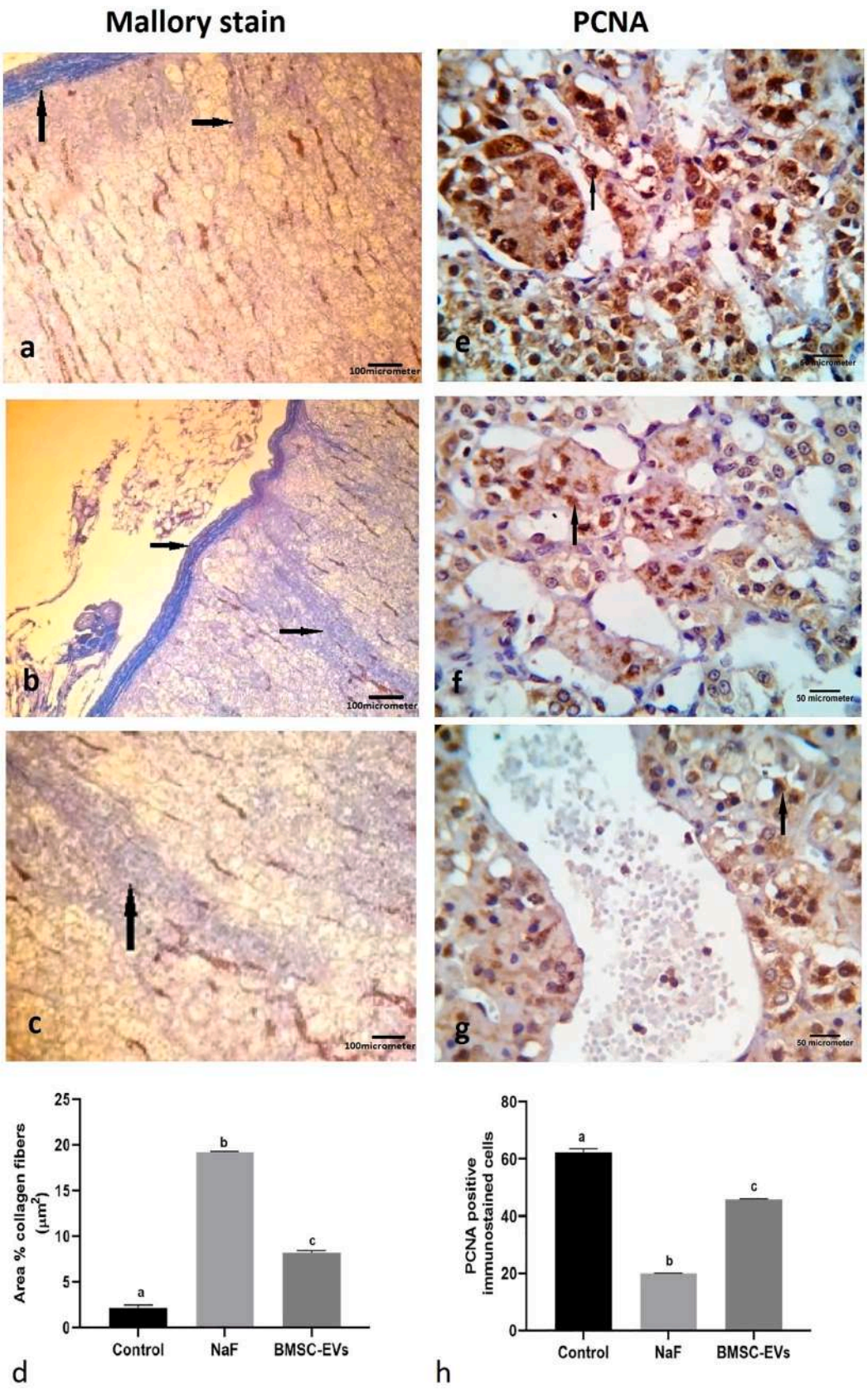

(caption on next page)

Fig. 5. Mallory trichrome and proliferating cell nuclear antigen (PCNA) stained sections of adrenals of the study groups.
a Control group showing collagen fibers deposition in capsule and parenchyma of the adrenals (arrows). Mallory trichrome stain, × 200. b NaF treated group showing a marked collagen fibers deposition in capsule and parenchyma of the adrenals (arrows). Mallory trichrome stain, × 200. c BMSC-EVs treated group showing mild collagen fibers deposition (arrow). Mallory trichrome stain, × 200. d Effects of BMSC-EVs on area percent of collagen fibers deposition of the adrenals in the rat sodium fluoride (NaF)-induced adrenal toxicity model. Data are mean ± standard deviation, $n = 7$ but two rats expired in NaF group. Bars not sharing the common superscript letters differ significantly at $P < 0.001$ by one-way ANOVA test followed by post hoc Bonferroni's multiple comparisons test. e Control group showing a positive immunostaining (a brown nuclear reaction) in most of the parenchymal cells of the adrenals (arrow) (Avidine biotin peroxidase stain with H× counter stain × 400). f NaF treated group showing few immunopositive parenchymal cells of the adrenals (arrow) for PCNA (Avidine biotin peroxidase stain with H× counter stain × 400). g BMSC-EVs treated group showing a positive immunostaining in most of the parenchymal cells of the adrenals (arrow) (Avidine biotin peroxidase stain with H× counter stain × 400). h Effects of BMSC-EVs on the mean number of adrenal PCNA immunostaining of the adrenals in the rat sodium fluoride (NaF)-induced adrenal toxicity model. Data are mean ± standard deviation, $n = 7$ but two rats expired in NaF group. Bars not sharing the common superscript letters differ significantly at $P < 0.001$ by Welch's ANOVA followed by post hoc Tamhane's T2 multiple comparisons test. (For interpretation of the references to colour in this figure legend, the reader is referred to the web version of this article.)

[12,66,67]. We can clarify these conflicting reports by the longer duration and the higher dose of fluoride in our study in comparison with these studies.

In conclusion, fluoride interfered with steroid biosynthesis and negatively influenced adrenals structures. BMSC-EVs mitigated the toxic effects of NaF and reprogramed injured adrenal cells by activating regenerative processes, thus restoring the functional and histological structure. Application of BMSC-EVs, a cell-free therapy, as a regeneration medicine opens novel perspectives for patients with corticosteroids deficiency disorders in the clinical practices.

Declaration of competing interest

The authors report no declaration of competing interest.

References

[1] P.W. Harvey, Adrenocortical endocrine disruption, J. Steroid Biochem. Mol. Biol. 155 (2016) 199–206, https://doi.org/10.1016/j.jsbmb.2014.10.009.

[2] J.C. Buckingham, The hypothalamo-pituitary-adrenocortical axis: endocrinology, pharmacology, pathophysiology, and developmental effects, in: P.W. Harvey, D. J. Everett, C. Springall (Eds.), Adrenal Toxicol. Organ Toxicol. Ser., Informa healthcare, New York (NY), 2009, pp. 77–107.

[3] P.W. Harvey, Toxic responses of the adrenal cortex, in: C.A. McQueen (Ed.), Compr. Toxicol, 3rd ed., Acadmeic Press, Elsevier Inc, 2018, pp. 165–182.

[4] J.P. Hinson, P.W. Raven, Effects of endocrine-disrupting chemicals on adrenal function, Best Pract. Res. Clin. Endocrinol. Metab. 20 (2006) 111–120, https://doi.org/10.1016/j.beem.2005.09.006.

[5] A. Inomata, H. Sasano, Practical approaches for evaluating adrenal toxicity in nonclinical safety assessment, J. Toxicol. Pathol. 28 (2015) 125–132, https://doi.org/10.1293/tox.2015-0025.

[6] J. Ameeramja, A. Raghunath, E. Perumal, Tamarind seed coat extract restores fluoride-induced hematological and biochemical alterations in rats, Environ. Sci. Pollut. Res. Int. 25 (2018) 26157–26166, https://doi.org/10.1007/s11356-018-2667-x.

[7] J. Fawell, K. Bailey, J. Chilton, E. Dahi, Y. Magara, Fluoride in drinking-water, IWA publishing, London, UK, 2006.

[8] J. Doull, K. Boekelheide, J.V. Farishian, Isaacson R.L. BG, J.B. Klotz, H. Limeback Kumar, C. Poole, J.E. Puzas, N.-M. Reed, K.M. Thiessen, T.F. Webster, N. R.C. of the N.A. Committee on Fluoride in Drinking Water, Board on Environmental Studies and Toxicology, Division on Earth and Life Studies, Fluoride in drinking water: a scientific review of EPA's standards, The National Academies Press, Washington, DC, USA, 2006.

[9] S.A.S. Moimaz, O. Saliba, L.B. Marques, C.A.S. Garbin, N.A. Saliba, Dental fluorosis and its influence on children's life, Braz. Oral Res. 29 (2015) S1806–83242015000100210, https://doi.org/10.1590/1807-3107BOR-2015.vol29.0014.

[10] G.B. Reddy, A.L. Khandare, P.Y. Reddy, G.S. Rao, N. Balakrishna, I. Srivalli, Antioxidant defense system and lipid peroxidation in patients with skeletal fluorosis and in fluoride-intoxicated rabbits, Toxicol. Sci. 72 (2003) 363–368, https://doi.org/10.1093/toxsci/kfg030.

[11] S.L. Choubisa, Status of fluorosis in animals, Proc. Natl. Acad. Sci. India Sect. B Biol. Sci. 82 (2012) 331–339, https://doi.org/10.1007/s40011-012-0026-0.

[12] P. Mehta, K.B. Singh, Drinking water toxicity of sodium fluoride in steroid producing glands and antioxidant ascorbate defense system in albino rats (*Rattus norvegicus*), J. Environ. Anal. Toxicol. 02 (2012), https://doi.org/10.4172/2161-0525.1000123.

[13] M. Skórka-Majewicz, M. Goschorska, W. Żwierełło, I. Baranowska-Bosiacka, D. Styburski, P. Kapczuk, I. Gutowska, Effect of fluoride on endocrine tissues and their secretory functions – review, Chemosphere. 260 (2020) 127565, https://doi.org/10.1016/j.chemosphere.2020.127565.

[14] C. Hu, L. Li, The application of resveratrol to mesenchymal stromal cell-based regenerative medicine, Stem Cell Res Ther 10 (2019) 307, https://doi.org/10.1186/s13287-019-1412-9.

[15] L. Barkholt, E. Flory, V. Jekerle, S. Lucas-Samuel, P. Ahnert, L. Bisset, D. Büscher, W. Fibbe, A. Foussat, M. Kwa, O. Lantz, R. Mačiulaitis, T. Palomäki, C.K. Schneider, L. Sensebé, G. Tachdjian, K. Tarte, L. Tosca, P. Salmikangas, Risk of tumorigenicity in mesenchymal stromal cell-based therapies–bridging scientific observations and regulatory viewpoints, Cytotherapy. 15 (2013) 753–759, https://doi.org/10.1016/j.jcyt.2013.03.005.

[16] J. Boltze, A. Arnold, P. Walczak, J. Jolkkonen, L. Cui, D.-C. Wagner, The dark side of the force - constraints and complications of cell therapies for stroke, Front. Neurol. 6 (2015) 155, https://doi.org/10.3389/fneur.2015.00155.

[17] J.A. Heslop, T.G. Hammond, I. Santeramo, A. Tort Piella, I. Hopp, J. Zhou, R. Baty, E.I. Graziano, B. Proto Marco, A. Caron, P. Sköld, P.W. Andrews, M.A. Baxter, D. C. Hay, J. Hamdam, M.E. Sharpe, S. Patel, D.R. Jones, J. Reinhardt, E.H.J. Danen, U. Ben-David, G. Stacey, P. Björquist, J. Piner, J. Mills, C. Rowe, G. Pellegrini, S. Sethu, D.J. Antoine, M.J. Cross, P. Murray, D.P. Williams, N.R. Kitteringham, C. E.P. Goldring, B.K. Park, Concise review: workshop review: understanding and assessing the risks of stem cell-based therapies, Stem Cells Transl. Med. 4 (2015) 389–400, https://doi.org/10.5966/sctm.2014-0110.

[18] I.A. Isakova, C. Lanclos, J. Bruhn, M.J. Kuroda, K.C. Baker, V. Krishnappa, D. G. Phinney, Allo-reactivity of mesenchymal stem cells in rhesus macaques is dose and haplotype dependent and limits durable cell engraftment in vivo, PLoS One 9 (2014), e87238, https://doi.org/10.1371/journal.pone.0087238.

[19] J.W. Jung, M. Kwon, J.C. Choi, J.W. Shin, I.W. Park, B.W. Choi, J.Y. Kim, Familial occurrence of pulmonary embolism after intravenous, adipose tissue-derived stem cell therapy, Yonsei Med. J. 54 (2013) 1293–1296, https://doi.org/10.3349/ymj.2013.54.5.1293.

[20] F. Collino, M. Pomatto, S. Bruno, R.S. Lindoso, M. Tapparo, W. Sicheng, P. Quesenberry, G. Camussi, Exosome aand microvesicle-enriched fractions isolated from mesenchymal stem cells by gradient separation showed different molecular signatures and functions on renal tubular epithelial cells, Stem Cell Rev. Reports. 13 (2017) 226–243, https://doi.org/10.1007/s12015-016-9713-1.

[21] F. Laso-García, J. Ramos-Cejudo, F.J. Carrillo-Salinas, L. Otero-Ortega, A. Feliú, M. Gómez-de Frutos, M. Mecha, E. Díez-Tejedor, C. Guaza, M. Gutiérrez-Fernández, Therapeutic potential of extracellular vesicles derived from human mesenchymal stem cells in a model of progressive multiple sclerosis, PLoS One 13 (2018), e0202590, https://doi.org/10.1371/journal.pone.0202590.

[22] M. Riazifar, M.R. Mohammadi, E.J. Pone, A. Yeri, C. Lässer, A.I. Segaliny, L. L. McIntyre, G.V. Shelke, E. Hutchins, A. Hamamoto, E.N. Calle, R. Crescitelli, W. Liao, V. Pham, Y. Yin, J. Jayaraman, J.R.T. Lakey, C.M. Walsh, K. Van Keuren-Jensen, J. Lotvall, W. Zhao, Stem cell-derived exosomes as nanotherapeutics for autoimmune and neurodegenerative disorders, ACS Nano 13 (2019) 6670–6688, https://doi.org/10.1021/acsnano.9b01004.

[23] M. Nawaz, F. Fatima, K.C. Vallabhaneni, P. Penfornis, H. Valadi, K. Ekström, S. Kholia, J.D. Whitt, J.D. Fernandes, R. Pochampally, J.A. Squire, G. Camussi, Extracellular vesicles: evolving factors in stem cell biology, Stem Cells Int. 2016 (2016) 1–17, https://doi.org/10.1155/2016/1073140.

[24] Y.J. Yoon, O.Y. Kim, Y.S. Gho, Extracellular vesicles as emerging intercellular communicasomes, BMB Rep. 47 (2014) 531–539, https://doi.org/10.5483/bmbrep.2014.47.10.164.

[25] E.R. Abels, X.O. Breakefield, Introduction to extracellular vesicles: biogenesis, rna cargo selection, content, release, and uptake, Cell. Mol. Neurobiol. 36 (2016) 301–312, https://doi.org/10.1007/s10571-016-0366-z.

[26] C. Théry, K.W. Witwer, E. Aikawa, M.J. Alcaraz, J.D. Anderson, R. Andriantsitohaina, A. Antoniou, T. Arab, F. Archer, G.K. Atkin-Smith, D.C. Ayre, J.-M. Bach, D. Bachurski, H. Baharvand, L. Balaj, S. Baldacchino, N.N. Bauer, A. A. Baxter, M. Bebawy, C. Beckham, A. Bedina Zavec, A. Benmoussa, A.C. Berardi, P. Bergese, E. Bielska, C. Blenkiron, S. Bobis-Wozowicz, E. Boilard, W. Boireau, A. Bongiovanni, F.E. Borràs, S. Bosch, C.M. Boulanger, X. Breakefield, A.M. Breglio, M.Á. Brennan, D.R. Brigstock, A. Brisson, M.L. Broekman, J.F. Bromberg, P. Bryl-Górecka, S. Buch, A.H. Buck, D. Burger, S. Busatto, D. Buschmann, B. Bussolati, E. I. Buzás, J.B. Byrd, G. Camussi, D.R. Carter, S. Caruso, L.W. Chamley, Y.-T. Chang, C. Chen, S. Chen, L. Cheng, A.R. Chin, A. Clayton, S.P. Clerici, A. Cocks, E. Cocucci,

R.J. Coffey, A. Cordeiro-da-Silva, Y. Couch, F.A. Coumans, B. Coyle, R. Crescitelli, M.F. Criado, C. D'Souza-Schorey, S. Das, A. Datta Chaudhuri, P. de Candia, E.F. De Santana, O. De Wever, H.A. Del Portillo, T. Demaret, S. Deville, A. Devitt, B. Dhondt, D. Di Vizio, L.C. Dieterich, V. Dolo, A.P. Dominguez Rubio, M. Dominici, M.R. Dourado, T.A. Driedonks, F.V. Duarte, H.M. Duncan, R. M. Eichenberger, K. Ekström, S. El Andaloussi, C. Elie-Caille, U. Erdbrügger, J. M. Falcón-Pérez, F. Fatima, J.E. Fish, M. Flores-Bellver, A. Försönits, A. Frelet-Barrand, F. Fricke, G. Fuhrmann, S. Gabrielsson, A. Gámez-Valero, C. Gardiner, K. Gärtner, R. Gaudin, Y.S. Gho, B. Giebel, C. Gilbert, M. Gimona, I. Giusti, D. C. Goberdhan, A. Görgens, S.M. Gorski, D.W. Greening, J.C. Gross, A. Gualerzi, G. N. Gupta, D. Gustafson, A. Handberg, R.A. Haraszti, P. Harrison, H. Hegyesi, A. Hendrix, A.F. Hill, F.H. Hochberg, K.F. Hoffmann, B. Holder, H. Holthofer, B. Hosseinkhani, G. Hu, Y. Huang, V. Huber, S. Hunt, A.G.-E. Ibrahim, T. Ikezu, J. M. Inal, M. Isin, A. Ivanova, H.K. Jackson, S. Jacobsen, S.M. Jay, M. Jayachandran, G. Jenster, L. Jiang, S.M. Johnson, J.C. Jones, A. Jong, T. Jovanovic-Talisman, S. Jung, R. Kalluri, S.-I. Kano, S. Kaur, Y. Kawamura, E.T. Keller, D. Khamari, E. Khomyakova, A. Khvorova, P. Kierulf, K.P. Kim, T. Kislinger, M. Klingeborn, D. J. Klinke, M. Kornek, M.M. Kosanović, Á.F. Kovács, E.-M. Krämer-Albers, S. Krasemann, M. Krause, I.V. Kurochkin, G.D. Kusuma, S. Kuypers, S. Laitinen, S. M. Langevin, L.R. Languino, J. Lannigan, C. Lässer, L.C. Laurent, G. Lavieu, E. Lázaro-Ibáñez, S. Le Lay, M.-S. Lee, Y.X.F. Lee, D.S. Lemos, M. Lenassi, A. Leszczynska, I.T. Li, K. Liao, S.F. Libregts, E. Ligeti, R. Lim, S.K. Lim, A. Linē, K. Linnemannstöns, A. Llorente, C.A. Lombard, M.J. Lorenowicz, Á.M. Lörincz, J. Lötvall, J. Lovett, M.C. Lowry, X. Loyer, Q. Lu, B. Lukomska, T.R. Lunavat, S. L. Maas, H. Malhi, A. Marcilla, J. Mariani, J. Mariscal, E.S. Martens-Uzunova, L. Martin-Jaular, M.C. Martinez, V.R. Martins, M. Mathieu, S. Mathivanan, M. Maugeri, L.K. McGinnis, M.J. McVey, D.G. Meckes, K.L. Meehan, I. Mertens, V. R. Minciacchi, A. Möller, M. Møller Jørgensen, A. Morales-Kastresana, J. Morhayim, F. Mullier, M. Muraca, L. Musante, V. Mussack, D.C. Muth, K. H. Myburgh, T. Najrana, M. Nawaz, I. Nazarenko, P. Nejsum, C. Neri, T. Neri, R. Nieuwland, L. Nimrichter, J.P. Nolan, E.N. Nolte-'t Hoen, N. Noren Hooten, L. O'Driscoll, T. O'Grady, A. O'Loghlen, T. Ochiya, M. Olivier, A. Ortiz, L.A. Ortiz, X. Osteikoetxea, O. Østergaard, M. Ostrowski, J. Park, D.M. Pegtel, H. Peinado, F. Perut, M.W. Pfaffl, D.G. Phinney, B.C. Pieters, R.C. Pink, D.S. Pisetsky, E. Pogge von Strandmann, I. Polakovicova, I.K. Poon, B.H. Powell, I. Prada, L. Pulliam, P. Quesenberry, A. Radeghieri, R.L. Raffai, S. Raimondo, J. Rak, M. I. Ramirez, G. Raposo, M.S. Rayyan, N. Regev-Rudzki, F.L. Ricklefs, P.D. Robbins, D.D. Roberts, S.C. Rodrigues, E. Rohde, S. Rome, K.M. Rouschop, A. Rughetti, A. E. Russell, P. Saá, S. Sahoo, E. Salas-Huenuleo, C. Sánchez, J.A. Saugstad, M. J. Saul, R.M. Schiffelers, R. Schneider, T.H. Schøyen, A. Scott, E. Shahaj, S. Sharma, O. Shatnyeva, F. Shekari, G.V. Shelke, A.K. Shetty, K. Shiba, P.R.-M. Siljander, A. M. Silva, A. Skowronek, O.L. Snyder, R.P. Soares, B.W. Sódar, C. Soekmadji, J. Sotillo, P.D. Stahl, W. Stoorvogel, S.L. Stott, E.F. Strasser, S. Swift, H. Tahara, M. Tewari, K. Timms, S. Tiwari, R. Tixeira, M. Tkach, W.S. Toh, R. Tomasini, A. C. Torrecilhas, J.P. Tosar, V. Toxavidis, L. Urbanelli, P. Vader, B.W. van Balkom, S. G. van der Grein, J. Van Deun, M.J. van Herwijnen, K. Van Keuren-Jensen, G. van Niel, M.E. van Royen, A.J. van Wijnen, M.H. Vasconcelos, I.J. Vechetti, T.D. Veit, L. J. Vella, É. Velot, F.J. Verweij, B. Vestad, J.L. Viñas, T. Visnovitz, K.V. Vukman, J. Wahlgren, D.C. Watson, M.H. Wauben, A. Weaver, J.P. Webber, V. Weber, A. M. Wehman, D.J. Weiss, J.A. Welsh, S. Wendt, A.M. Wheelock, Z. Wiener, L. Witte, J. Wolfram, A. Xagorari, P. Xander, J. Xu, X. Yan, M. Yáñez-Mó, H. Yin, Y. Yuana, V. Zappulli, J. Zarubova, V. Žėkas, J.-Y. Zhang, Z. Zhao, L. Zheng, A.R. Zheutlin, A. M. Zickler, P. Zimmermann, A.M. Zivkovic, D. Zocco, E.K. Zuba-Surma, Minimal information for studies of extracellular vesicles 2018 (MISEV2018): a position statement of the International Society for Extracellular Vesicles and update of the MISEV2014 guidelines, J. Extracell. Vesicles. 7 (2018) 1535750, https://doi.org/10.1080/20013078.2018.1535750.

[27] G. van Niel, G. D'Angelo, G. Raposo, Shedding light on the cell biology of extracellular vesicles, Nat. Rev. Mol. Cell Biol. 19 (2018) 213–228, https://doi.org/10.1038/nrm.2017.125.

[28] A. Alhadlaq, J.J. Mao, Mesenchymal stem cells: isolation and therapeutics, Stem Cells Dev. 13 (2004) 436–448, https://doi.org/10.1089/scd.2004.13.436.

[29] S. Schachtele, C. Clouser, J. Ho, Markers & Methods to Verify Mesenchymal Stem Cell Identity, Potency, & Quality Minireviews R&D Syst 10, 2013.

[30] P.K. Wallace, K.A. Muirhead, Cell tracking 2007: a proliferation of probes and applications, Immunol. Investig. 36 (2007) 527–561, https://doi.org/10.1080/08820130701812584.

[31] S. Gatti, S. Bruno, M.C. Deregibus, A. Sordi, V. Cantaluppi, C. Tetta, G. Camussi, Microvesicles derived from human adult mesenchymal stem cells protect against ischaemia-reperfusion-induced acute and chronic kidney injury, Nephrol. Dial. Transplant. 26 (2011) 1474–1483, https://doi.org/10.1093/ndt/gfr015.

[32] J. Ameeramja, V.V. Kanagaraj, E. Perumal, Protocatechuic acid methyl ester modulates fluoride induced pulmonary toxicity in rats, Food Chem. Toxicol. 118 (2018) 235–244, https://doi.org/10.1016/j.fct.2018.05.031.

[33] P. Ekambaram, T. Namitha, S. Bhuvaneswari, S. Aruljothi, D. Vasanth, M.J. F. Saravanakumar, Therapeutic efficacy of *Tamarindus indica* (L) to protect against fluoride-induced oxidative stress in the liver of female rats, Fluoride 43 (2010).

[34] J. Yang, X.-X. Liu, H. Fan, Q. Tang, Z.-X. Shou, D.-M. Zuo, Z. Zou, M. Xu, Q.-Y. Chen, Y. Peng, S.-J. Deng, Y.-J. Liu, Extracellular vesicles derived from bone marrow mesenchymal stem cells protect against experimental colitis via attenuating colon inflammation, oxidative stress and apoptosis, PLoS One 10 (2015), e0140551, https://doi.org/10.1371/journal.pone.0140551.

[35] M.B. Leal Filho, R.C. Morandin, A.R. de Almeida, E.C. Cambiucci, K. Metze, G. Borges, J.A.R. Gontijo, Hemodynamic parameters and neurogenic pulmonary edema following spinal cord injury: an experimental model, Arq. Neuropsiquiatr. 63 (2005) 990–996, doi:/S0004-282X2005000600016.

[36] K.J. Livak, T.D. Schmittgen, Analysis of relative gene expression data using real-time quantitative PCR and the 2−ΔΔCT method, Methods. 25 (2001) 402–408, https://doi.org/10.1006/meth.2001.1262.

[37] J.D. Bancroft, C. Layton, The hematoxylin and eosin, in: S.K. Suvarna, C. Layton, J. D. Bancroft (Eds.), Bancroft's Theory Pract. Histol. Tech, 8th ed., Elsevier, Philadelphia, 2019, pp. 126–138.

[38] C. Layton, J.D. Bancroft, Carbohydrates, in: S. Suvarna, L. C. J. Bancroft (Eds.), Bancroft's Theory Pract. Histol. Tech., 8th ed., Elsevier, Philadelphia, 2019: pp. 76–197.

[39] J. Bancroft, C. Layton, Connective tissue and other mesenchymal tissues with their stains, in: Bancroft's Theory Pract. Histol. Tech, 8th ed., Elsevier, Phialdelphia, 2019, pp. 153–175.

[40] T. Sanderson, G. Wild, A.M. Cull, J. Marston, G. Zardin, Immunohistochemical and immunofluoresent techniques, in: Bancroft's Theory Pract. Histol. Tech., 8th, Elsevier, Phialdelphia, 2019, pp. 337–396.

[41] V.K. Bharti, A. Giri, K. Kumar, Fluoride sources, toxicity and its amelioration: a review, Ann. Environ. Sci. Toxicol. 2 (2018).

[42] H. Sies, On the history of oxidative stress: concept and some aspects of current development, Curr. Opin. Toxicol. 7 (2018) 122–126, https://doi.org/10.1016/j.cotox.2018.01.002.

[43] P. Jaiswal, M. Mandal, A. Mishra, Effect of hesperidin on fluoride-induced neurobehavioral and biochemical changes in rats, J. Biochem. Mol. Toxicol. 34 (2020), e22575, https://doi.org/10.1002/jbt.22575.

[44] G.H.N. Miranda, B.A.Q. Gomes, L.O. Bittencourt, W.A.B. Aragão, L.S. Nogueira, A. S. Dionizio, M.A.R. Buzalaf, M.C. Monteiro, R.R. Lima, Chronic exposure to sodium fluoride triggers oxidative biochemistry misbalance in mice: effects on peripheral blood circulation, Oxidative Med. Cell. Longev. 2018 (2018) 8379123, https://doi.org/10.1155/2018/8379123.

[45] S. Keshtkar, N. Azarpira, M.H. Ghahremani, Mesenchymal stem cell-derived extracellular vesicles: novel frontiers in regenerative medicine, Stem Cell Res Ther 9 (2018) 63, https://doi.org/10.1186/s13287-018-0791-7.

[46] V. Bodart-Santos, L.R.P. de Carvalho, M.A. de Godoy, A.F. Batista, L.M. Saraiva, L. G. Lima, C.A. Abreu, F.G. De Felice, A. Galina, R. Mendez-Otero, S.T. Ferreira, Extracellular vesicles derived from human Wharton's jelly mesenchymal stem cells protect hippocampal neurons from oxidative stress and synapse damage induced by amyloid-β oligomers, Stem Cell Res Ther 10 (2019) 332, https://doi.org/10.1186/s13287-019-1432-5.

[47] A. Arukwe, Steroidogenic acute regulatory (StAR) protein and cholesterol side-chain cleavage (P450scc)-regulated steroidogenesis as an organ-specific molecular and cellular target for endocrine disrupting chemicals in fish, Cell Biol. Toxicol. 24 (2008) 527–540, https://doi.org/10.1007/s10565-008-9069-7.

[48] N.M. Khorram, T.R. Magee, C. Wang, M. Desai, M. Ross, O. Khorram, Maternal undernutrition programs offspring adrenal expression of steroidogenic enzymes, Reprod. Sci. 18 (2011) 931–940, https://doi.org/10.1177/1933719111404613.

[49] K. Peng, Y. Pan, J. Li, Z. Khan, M. Fan, H. Yin, C. Tong, Y. Zhao, G. Liang, C. Zheng, 11β-Hydroxysteroid dehydrogenase type 1(11β-HSD1) mediates insulin resistance through JNK activation in adipocytes, Sci. Rep. 6 (2016) 37160, https://doi.org/10.1038/srep37160.

[50] T. Yu, H. Xu, W. Wang, S. Li, Z. Chen, H. Deng, Determination of endogenous corticosterone in rodent's blood, brain and hair with LC-APCI-MS/MS, J. Chromatogr. B. Analyt. Technol. Biomed. Life Sci. 1002 (2015) 267–276, https://doi.org/10.1016/j.jchromb.2015.08.035.

[51] T.R. Webb, L. Chan, S.N. Cooray, M.E. Cheetham, J.P. Chapple, A.J.L. Clark, Distinct melanocortin 2 receptor accessory protein domains are required for melanocortin 2 receptor interaction and promotion of receptor trafficking, Endocrinology. 150 (2009) 720–726, https://doi.org/10.1210/en.2008-0941.

[52] J.A. Sebag, P.M. Hinkle, Opposite effects of the melanocortin-2 (MC2) receptor accessory protein MRAP on MC2 and MC5 receptor dimerization and trafficking, J. Biol. Chem. 284 (2009) 22641–22648, https://doi.org/10.1074/jbc.M109.022400.

[53] S.N. Cooray, A.J.L. Clark, Melanocortin receptors and their accessory proteins, Mol. Cell. Endocrinol. 331 (2011) 215–221, https://doi.org/10.1016/j.mce.2010.07.015.

[54] E.T. Everett, Fluoride's effects on the formation of teeth and bones, and the influence of genetics, J. Dent. Res. 90 (2011) 552–560, https://doi.org/10.1177/0022034510384626.

[55] A. Horii, K. Mitani, C. Masumura, A. Uno, T. Imai, Y. Morita, K. Takahashi, T. Kitahara, H. Inohara, Hippocampal gene expression, serum cortisol level, and spatial memory in rats exposed to hypergravity, J. Vestib. Res. 27 (2017) 209–215, https://doi.org/10.3233/VES-170521.

[56] L. Macho, R. Kvetnansky, M. Fickova, I.A. Popova, A. Grigoriev, Effects of exposure to space flight on endocrine regulations in experimental animals, Endocr. Regul. 35 (2001) 101–114. http://www.ncbi.nlm.nih.gov/pubmed/11563939.

[57] T.K. Das, A.K. Susheela, Effect of chronic fluoride toxicity on glucocorticoid levels in plasma and urine, Fluoride. 24 (1991) 23–28.

[58] J.K. Gjerstad, S.L. Lightman, F. Spiga, Role of glucocorticoid negative feedback in the regulation of HPA axis pulsatility, Stress. 21 (2018) 403–416, https://doi.org/10.1080/10253890.2018.1470238.

[59] K.J. Ioakim, G.I. Sydney, S.A. Paschou, Glucose metabolism disorders in patients with adrenal gland disorders: pathophysiology and management, Hormones (Athens) 19 (2020) 135–143, https://doi.org/10.1007/s42000-019-00147-z.

[60] G.A. Ueland, E.S. Husebye, Metabolic complications in adrenal insufficiency, in: V. Popovic, M. Korbonits (Eds.), Metab. Syndr. Consequent to Endocr. Disord, 1st ed., Front Horm Res, Karger, Basel, 2018, pp. 104–113, https://doi.org/10.1159/000486004.

[61] C. Grange, S. Tritta, M. Tapparo, M. Cedrino, C. Tetta, G. Camussi, M.F. Brizzi, Stem cell-derived extracellular vesicles inhibit and revert fibrosis progression in a mouse model of diabetic nephropathy, Sci. Rep. 9 (2019) 4468, https://doi.org/10.1038/s41598-019-41100-9.
[62] W. Strzalka, A. Ziemienowicz, Proliferating cell nuclear antigen (PCNA): a key factor in DNA replication and cell cycle regulation, Ann. Bot. 107 (2011) 1127–1140, https://doi.org/10.1093/aob/mcq243.
[63] S. Bruno, M. Tapparo, F. Collino, G. Chiabotto, M.C. Deregibus, R. Soares Lindoso, F. Neri, S. Kholia, S. Giunti, S. Wen, P. Quesenberry, G. Camussi, Renal regenerative potential of different extracellular vesicle populations derived from bone marrow mesenchymal stromal cells, Tissue Eng. Part A. 23 (2017) 1262–1273, https://doi.org/10.1089/ten.tea.2017.0069.
[64] Z.-Y. Zhang, Y.-P. Hou, X.-Y. Zou, X.-Y. Xing, G.-Q. Ju, L. Zhong, J. Sun, Oct-4 enhanced the therapeutic effects of mesenchymal stem cell-derived extracellular vesicles in acute kidney injury, Kidney Blood Press. Res. 45 (2020) 95–108, https://doi.org/10.1159/000504368.
[65] B. Zhang, M. Wang, A. Gong, X. Zhang, X. Wu, Y. Zhu, H. Shi, L. Wu, W. Zhu, H. Qian, W. Xu, HucMSC-exosome mediated-wnt4 signaling is required for cutaneous wound healing, Stem Cells 33 (2015) 2158–2168, https://doi.org/10.1002/stem.1771.
[66] E.L. McGown, J.W. Suttie, Mechanism of fluoride-induced hyperglycemia in the rat, Toxicol. Appl. Pharmacol. 40 (1977) 83–90, https://doi.org/10.1016/0041-008X(77)90119-3.
[67] Y.S. Cheon, V. DiStefano, Effect of sodium fluoride on catecholamine concentrations in tissues from developing rats, Toxicol. Appl. Pharmacol. 24 (1973) 468–473, https://doi.org/10.1016/0041-008X(73)90053-7.